Self-blockade of PD-L1 with bacteria-derived outer-membrane vesicle for enhanced cancer immunotherapy

*Jingmei Pan, Xilin Li, Binfen Shao, Funeng Xu, Xuehui Huang, Xing Guo*and Shaobing Zhou**

Dr. J. Pan, Dr. X. Li, Dr. F. Xu, Dr. X. Huang, Prof. X. Guo, Prof. S. Zhou

Key Laboratory of Advanced Technologies of Materials Ministry of Education, School of Materials Science and Engineering, Southwest Jiaotong University, Chengdu 610031, P. R. China.
E-mail: xingguo@swjtu.edu.cn and shaobingzhou@swjtu.edu.cn

B.Shao

School of Life Science and Engineering, Southwest Jiaotong University, Chengdu 610031, P. R. China.

Keywords: immune checkpoint, nanocarrier, outer-membrane vesicle, immunotherapy, immune response

The checkpoint inhibitor therapy that blocks the Programmed Death-1 (PD-1) and its major ligand PD-L1, has achieved encouraging clinical efficacy in certain cancers. However,

This article has been accepted for publication and undergone full peer review but has not been through the copyediting, typesetting, pagination and proofreading process, which may lead to differences between this version and the Version of Record. Please cite this article as doi: 10.1002/adma.202106307.

the binding of checkpoint inhibitors with other immune cells that express PD-L1 often results in a low response rate to the blockade and severe adverse effects. Herein, we developed a LyP1 polypeptide-modified outer-membrane vesicle (LOMV) loaded with a PD-1 plasmid to achieve self-blockade of PD-L1 in tumor cells. The nanocarriers accumulated in the tumor tissue through OMV-targeting ability and were internalized into the tumor cells via LyP1-mediated target, subsequently delivering PD-1 plasmid into the nucleus, leading to the expression of PD-1 by tumor cells. In addition, a magnetic particle chemiluminescence kit was developed to quantitatively detect the binding rate of PD-1/PD-L1. The self-expressed PD-1 bonded with the PD-L1 expressed by both autologous and neighboring tumor cells, achieving self-blockade. Simultaneously, the outer-membrane protein of LOMV recruited cytotoxic lymphocyte cells and natural killer cells to tumor tissues and stimulated them to secrete IFN-γ, improving the antitumor activity of the PD-1/PD-L1 self-blocking therapy.

Immunotherapies that block the immune checkpoints Programmed Death-1 (PD-1) and Programmed death ligand-1 (PD-L1) have revolutionized the approach to cancer treatment as they have achieved significant clinical efficacy in certain types of cancers.[1] PD-1 is upregulated on activated T cells to induce immune tolerance[2] whereas PD-L1 is frequently overexpressed on tumor cells and interacts with PD-1, inhibiting T cells and blocking the antitumor immune response.[3] PD-L1 monoclonal antibodies, which are currently approved

by the U.S. Food and Drug Administration (FDA) for inhibiting the interaction between PD-1 and PD-L1 to rescue the dysfunction of CTLs, have made substantial progress in treating some cancers.[4] However, some problems remain unresolved, including a low response rate (~20%) to blockade in patients and severe treatment-associated adverse effects related to the long half-life of these antibody drugs.[5] One of the main reasons for this is that these checkpoint inhibitors also bind with other immune cells that express PD-L1, including antigen-presenting cells, activated B cells, and macrophages,[3b,6] resulting in interference of the immune function. Therefore, selectively accumulating these checkpoint blockers in tumor tissue and subsequently concentrating their action on tumor-reactive effector cells are critical for improving the immunotherapeutic efficacy and decreasing systematic toxicity.

Nanoparticle-based drug delivery systems have been developed to deliver checkpoint inhibitors to tumor sites and ensure their constant release for enhancing both therapeutic efficacy and safety.[7] This nanoparticle-based approach can widely select multifunctional matrix materials, readily change their size and shape, and easily offer surface modifications with functional groups.[8] As such, nanoparticles can improve the local retention of immunotherapeutics and prevent them from diffusing into the blood circulation. Despite this, the efficacy of this single immune checkpoint blockade therapy remains unsatisfactory in various solid tumors. To improve its therapeutic effect, this theory needs to be combined with other therapeutic strategies, such as chemotherapy,[9] radiotherapy,[10] photothermal

therapy,[11] and photodynamic therapy.[7b,9] However, these combined strategies still incur the defects of traditional treatments, such as significant side-effects and limited efficacy. Therefore, the development of robust strategies for blocking PD-L1 to improve the response rates of cancers is significant.

Accordingly, in this study, we developed a LyP1 polypeptide-modified outer-membrane vesicle (LOMV) loaded with a PD-1 plasmid to achieve self-blockade of PD-L1 for enhanced cancer immunotherapy. As shown in **Figure 1**, first, *E. coli* was engineered to express the targeted polypeptide LyP1, followed by the extraction of LOMVs, which were used to encapsulate the PD-1 plasmid to obtain LyP1-OMVs@PD-1 (LOMV@PD-1) nanocarriers. Through intravenous injection, these nanocarriers were accumulated in tumor tissue through OMVs' target ability[12] and internalized into tumor cells via a LyP1-mediated target, subsequently delivering the PD-1 plasmid into the nucleus, leading to the expression of PD-1 by tumor cells. The self-expressed PD-1 bonded with the PD-L1 expressed by both autologous and neighboring tumor cells, achieving self-blockade of the PD-1/PD-L1 pathway. Consequently, CTLs were reactivated to eradicate cancer cells. At the same time, the outer-membrane protein component of OMVs recruited cytotoxic lymphocyte cells (CTLs) and natural killer (NK) cells to tumor tissues and stimulated them to secrete IFN-γ,[13] further improving the antitumor activity of the PD-1/PD-L1 self-blocking therapy. Moreover,

the OMVs differentiated CTLs into central memory T cells (Tcm), developing long-lasting immunity.

Lipopolysaccharide (LPS), also called endotoxin, is the main component of the outer membrane of gram-negative bacteria.[14] As the biologically active center of LPS, lipid A can cause a strong inflammatory response and regulate the immune response.[15] To reduce the toxicity of LPS, we used a K-12 W3110 *E. coli* strain with an inactivated gene-encoding lipid A acyltransferase.[13] Next, we constructed a plasmid that expresses LyP1 polypeptide with a CGNKRTRGC sequence, which was connected to cytolysin A (ClyA)[16] in *E. coli* via a flexible linker with SSSSGSSSSG sequence (**Figure S1** and **Figure S2**a, c). The plasmid ClyA-linker-LyP1 was verified by agarose gel electrophoresis (**Figure S2**b) and the Myc-tag protein expressed by genetically modified K-12 W3110 *E. coli* was validated by western blotting (**Figure 2**a). The OMVs of the engineered K-12 W3110 *E. coli* (LOMV) were extracted through ultrafiltration and centrifugation (**Figure S2**d). Transmission electron micrograph (TEM) images and dynamic light scattering (DLS) analysis showed that these LOMVs were approximately 136.9 nm in size with a spherical morphology (**Figure 2**b, c). In addition, there was no significant change in particle size and protein concentration when LOMVs were stored at 25 °C for 3 days and 4 °C for 7 days, indicating the suitable stability of the vesicles (**Figure S3**a-c). The expression of the LyP1 peptide in OMVs was confirmed by western blotting (**Figure 2**d).

To study the tumor-targeting ability of LOMV, we used 4T1 cells which has a low response rate to PD-1/PD-L1 therapy, fluorescein isothiocyanate (FITC)-labeled OMV was incubated with 4T1 cells and evaluated by fluorescence microscopy and flow cytometry. Both OMV and LOMV groups exhibited strong fluorescence intensity with prolonged co-incubation time (**Figure 2**e-g). As expected, LyP1 expression increased the cellular uptake of OMVs to some extent, showing an approximately 10% higher internalization rate due to the targeting ability of nine cyclic amino acid peptides (LyP1) to tumor.[17] Quartz crystal microbalance (QCM) was performed to further investigate the tumor-targeting efficiency.[18] Compared with OMV, the vibration frequency of the LOMV group was lower within the experimental time, indicating that LOMV bonded more easily with 4T1 cells (**Figure 2**h). In addition, live/dead staining and Alamar Blue assay showed negligible LOMV cytotoxicity (**Figure S4**a, b). The hemolysis rates of OMV and LOMV were less than 5% (**Figure S4**c, d), and no clotting was observed in the coagulation assay (**Figure S**4e). These results indicate that the engineered OMVs and LOMVs possessed suitable biocompatibility.

The pEGFP-N1-PD-1 plasmid, which expresses PD-1, was constructed (**Figure S5, S6**) and loaded into LOMV by electroporation. To filter out the optimum voltage condition, the expression of PD-1 at different voltages was detected by fluorescence and western blotting to evaluate the electrotransformation efficiency (**Figure S7**a, b). The results indicated that the fluorescence intensity and protein content of PD-1 were the highest at 600 V, reaching an

electrotransformation efficiency of 80% (**Figure S7**c). Thus, we chose 600 V as the electroporation voltage to prepare the PD-1 plasmid-loaded vesicles. After LOMV@PD-1 delivered the PD-1 plasmid into the nucleus of tumor cells, the expression of PD-1 with green fluorescence would occur. To evaluate PD-1 expression, 4T1 cells were treated with LOMV@PD-1 and tested by fluorescence microscopy and flow cytometry. Obvious fluorescence signals could be found within 72 h, illustrating the successful transfection of PD-1 plasmid through LOMV and the subsequent expression of PD-1 on 4T1 cells (**Figure 2**i, j), and most of the PD-1 was expressed on the cell membrane (**Figure S7**d). We further investigated PD-1 mRNA and protein expression in 4T1 cells after incubation with LOMV@PD-1 at different time points (**Figure 2**k-m). The results showed that the quantitative protein expression was consistent with the time-dependent fluorescence intensities, further confirming the successful transfection of PD-1 plasmid. As mRNA levels are only a part of the process of transcription, while proteins are a process of transcription translation and post-translational modification, the mRNA expression tendency of PD-1 is different from the result of western blotting.

To investigate whether the self-expressed PD-1 can bind to PD-L1 on the surface of 4T1 cells, we conducted an immunofluorescence assay. 4T1 cells with or without LOMV@PD-1 co-incubation was treated with the PD-L1 primary antibody and stained with 4′,6-diamidino-2-phenylindole (DAPI) sequentially. As shown in **Figure 3**a, no GFP green fluorescence was

observed in cells transfected without the PD-1 plasmid. In contrast, the overlapping orange fluorescence of green fluorescence and red fluorescence demonstrated that the newly expressed PD-1 could bind to the intrinsic PD-L1 of 4T1 cells (**Figure 3**b). Moreover, the corresponding relatively high Pearson's correlation coefficients (Rr) of green and red (0.85 ± 0.05) indicated a suitable combination of PD-1/PD-L1 (**Figure 3**c, d). The co-immunoprecipitation assay further confirmed the binding of PD-1 and PD-L1 (**Figure 3**e). These *in vitro* results indicated that the self-blockade of the PD-1/PD-L1 pathway can be realized by binding the self-expressed PD-1 with the intrinsic PD-L1 of tumor cells.

Next, we modified a commercial ELISA kit[19] by replacing PD-L1 antibody with PD-1 antibody to determine the absorbance of PD-1/PD-L1 conjugates (**Figure 3**f), which is proportional to the protein concentration. The maximum absorbance was determined at 48 h (**Figure 3**g). The most efficient combination of PD-1/PD-L1 at this point resulted from the highest PD-1 expression 48 h after plasmid transfection. Therefore, this modified ELISA kit can provide a time-dependent trend of PD-1/PD-L1 combination.

To quantitatively detect the concentration of PD-1/PD-L1 conjugates, we developed a magnetic particle-based chemiluminescence kit according to Chemiluminescentimmunoassay (CLIA)[20] (**Figure 3**h). The kit was stable at 4 °C and 37 °C for 7 days (**Figure S8**a). Then, 4T1 cells were treated with LOMV@PD-1 and the protein concentration of PD-1/PD-L1

conjugates was tested using this kit. The protein concentration of PD-1/PD-L1 conjugates detected by the chemiluminescence test showed a similar time-dependent trend compared to the modified ELISA kit, confirming the validity and reliability of the chemiluminescence kit. The highest binding rate at 48 h (**Figure 3**i and **Figure S8**b) was mainly attributed to the highest expression of PD-1 at the same time point after transfection with the PD-1 plasmid (**Figure 2**i). To calculate the self-blockade rate of PD-1/PD-L1, the PD-L1 concentration was detected by ELISA. The PD-L1 expression increased over time, which was due to the gradual proliferation of tumor, and the self-blockade rate became as high as 42% (**Figure 3**j and **Figure S8**c). In addition, there was a negligible difference in the PD-L1 concentration of the cells with and without LOMV@PD-1 treatment, indicating that the PD-1 plasmid-loaded OMV did not affect PD-L1 expression.

We used an *in vivo* imaging system to observe LOMV biodistribution after a systemic administration. The vesicles were loaded with Cy5.5 and intravenously injected into 4T1 tumor-bearing mice. Both OMV and LOMV displayed significant accumulation at the tumor site after 24 h of administration (**Figure 4**a), whereas the fluorescence intensity of LOMV was 1.5-fold higher than that of OMV (**Figure S9**a), indicating the effective tumor-targeting ability of LyP1. The *ex vivo* fluorescence of the excised tissues further illustrated the enhanced tumor accumulation of LOMV (**Figure 4**b, c).

An *in vivo* antitumor study was conducted on 4T1 breast tumor-bearing BALB/c mice. When the tumor volume reached 50 mm^3, the mice were intravenously injected with various formulations, except for the PD-L1 monoclonal antibody group (anti-PD-L1), which was intraperitoneally injected[21] (**Figure 4**d). Treating the mice with LOMV@PD-1 resulted in significant tumor inhibition, with a tumor growth inhibition (TGI) of 74%, which was approximately 2.5-fold higher than that of the anti-PD-L1 group (**Figure 4**e-g and **Figure S9**b, c). Compared to LOMV@PD-1, the OMV@PD-1 group without LyP1 modification or the LOMV group without PD-1 plasmid was less effective for tumor suppression. These results also indicate that the LOMV nanocarrier can maintain the biological activity of the PD-1 plasmid and effectively deliver it to the tumor cells. The low therapeutic efficacy of PD-L1 antibody can be ascribed to its limited penetration into the tissues and tumors.[22] As a main indicator of systemic toxicity, the body weight of the mice was monitored for 30 days. No obvious weight loss was observed in any treatment group (**Figure 4**h). Owing to the remarkable tumor inhibition, the survival rate of the mice was significantly prolonged when treated with LOMV@PD-1 (**Figure 4**i). To further study the antitumor activity, hematoxylin and eosin (H&E), Ki67, and terminal deoxynucleotidyl transferase dUTP nick end labeling (TUNEL) staining were performed (**Figure 4**j). Compared to other groups, LOMV@PD-1 presented significant nuclear condensation and fragmentation in H&E images and possessed the fewest Ki67-positive proliferating cells and maximum TUNEL-apoptotic cells, implying

enhanced therapeutic efficiency.[23] In addition, the blood biochemical indexes and routine blood tests demonstrated that the various formulations had no adverse effects on liver and kidney functions (**Figure S10**a, b). The H&E staining of the normal organs further confirmed the safety of the treatment (**Figure S10**c), illustrating the potential application of an LOMV as a delivery system.

The antitumor mechanism of LOMV@PD-1 was further analyzed. First, we investigated whether the self-blockade of the PD-1/PD-L1 pathway *in vivo* was similar to the *in vitro* result. Given the complexity of the *in vivo* environment, quantitative real-time polymerase chain reaction (qPCR) was conducted to detect the mRNA levels of PD-1 and PD-L1 in plasma and tumor tissues, respectively.[19]

There was a negligible difference in the plasma PD-1 mRNA levels between the groups. In contrast, PD-1 levels were higher in the plasmid-loaded OMV groups than those in the other groups. In particular, the LOMV@PD-1 group showed the highest expression of PD-1 in tumor tissues, indicating that the PD-1 plasmid was effectively delivered to the tumor cells by LOMV, resulting in successful transfection and self-expression of PD-1 (**Figure 5**a). As shown in **Figure 5**b, mice treated with LOMV@PD-1 had the lowest plasma PD-L1 mRNA levels. In addition, PD-L1 protein expression in plasma was consistent with the mRNA levels (**Figure 5**c). Some studies have shown that the low efficiency of PD-1/PD-L1 treatment is

related to an increase in plasma PD-L1 levels.[24] The lowest PD-L1 levels in plasma indicated that the self-blockade therapy with LOMV@PD-1 could enhance the therapeutic effect. A Pearson correlation coefficient analysis[19] indicated a positive correlation between PD-L1 concentration in plasma and tumor volume (correlation coefficient: 0.9576); namely, an increased PD-L1 expression in plasma resulted in a larger tumor volume, which also indicates that PD-L1 can be used as a therapeutic prognostic marker[24a] (**Figure 5**d).

Owing to the wide expression of PD-L1 by immune cells, including T cells, NK cells, and macrophages in the tumor microenvironment, PD-L1 expression in the tumor tissues was not decreased in the LOMV@PD-1 group (**Figure 5**e). In addition, these immune cells could be recruited to the tumor site by LOMV as potential IFN-γ producer. After treatment with LOMV@PD-1, two STING-related pathway proteins were slightly unregulated, indicating that this might be another potential pathway to increase the IFN-γ (**Figure S8**d, e). IFN-γ production could activate interferon regulatory factor 1 through JAK-STAT signal,[25] resulting in an increase in PD-L1 levels.[4,26] Consequently, the recruited immune cells could also induce the PD-L1 expression after the treatment group produced an immune response. This explains why the PD-L1 expression in the tumor tissues of the treatment group was higher than that in the saline group.

To quantitatively detect the binding of PD-L1 and PD-1 *in vivo*, we used a magnetic particle chemiluminescence kit to measure the concentration of PD-L1/PD-1 conjugates. The results showed that the blocking rate of LOMV@PD-1 reached 94.7%, which was 1.90 and 1.69 times the values achieved by the anti-PD-L1 group and anti-PD-L1+LOMV group, respectively, indicating a higher blocking effect when PD-L1 was combined with the self-expressed PD-1 (**Figure 5**f). The combination of PD-L1 and PD-1 was further verified by an immunofluorescence analysis. The LOMV@PD-1 group showed the highest superposition of green and red fluorescence, indicating the excellent combination of self-expressed PD-1 and intrinsic PD-L1 in tumor cells (**Figure 5**g). Interestingly, almost no T cells or macrophages bind with PD-1 after treatment. This further indicated that LOMV@PD-1 could successfully block the PD-1/PD-L1 of tumor cells and consequently inhibit the interaction of the PD-1 on tumor cells with the PD-L1 on the immune cells (**Figure S11**a, b). The self-blockade of PD-L1 *in vivo* is key for the enhanced antitumor efficacy in the LOMV@PD-1 group because it can reactivate CTLs to eradicate the cancer cells.

The other mechanism of the antitumor effect was analyzed from the recruitment of immune cells owing to the outer-membrane protein component of OMVs.[13] To validate this, we examined the number of CTLs and NK cells and IFN-γ levels in tumor tissue. Flow cytometry analysis of the number of NK cells at the end of the treatment showed that the LOMV@PD-1 group had the highest expression of $CD49b^+$ NK cells (**Figure 6**a, b). In

addition to inducing innate immunity, OMVs can also activate CTLs by promoting the maturation of dendritic cells (DCs).[27] As expected, the mice treated with LOMV@PD-1 possessed the highest expression of $CD80^+CD86^+$ DCs (**Figure 6**c, d), indicating the maximum amount of mature DCs in this group. Accordingly, the number of $CD8^+$ T cells was detected in the different groups. Despite the slight increase in infiltrating $CD8^+$ T cells into the tumor by anti-PD-L1,[22] the efficiency was far less than that of the LOMV@PD-1 group, which was 1.7 higher than that of the anti-PD-L1 group (**Figure S12**a and **Figure 6**f, g). In addition, LOMV@PD-1 could also increase the number of $CD4^+$ T cells, further indicating the recruitment of immune cells by LOMV.

Immunofluorescence staining further confirmed the highest expression of $CD49b^+$ NK cells and $CD4^+$ and $CD8^+$ T cells in the LOMV@PD-1 group (**Figure 6**e). These results indicate that LOMV@PD-1 could recruit CTLs and NK cells to reach tumor tissues, improve the tumor microenvironment, and inhibit the tumor formation by secreting IFN-γ. To prove this, qPCR and ELISA were used to detect IFN-γ expression in plasma and tumor tissues. LOMV@PD-1 induced the highest expression of IFN-γ in tumor tissues and the lowest expression of IFN-γ in plasma (**Figure 6**h-j and **Figure S8**f), indicating that the CTLs and NK cells recruited to the tumor tissues produced considerable IFN-γ. IFN-γ can induce the PD-L1 expression[26b] in tumor microenvironment cells while suppressing the tumor.[28] In our study, even if IFN-γ promoted the production of "harmful" PD-L1, LOMV@PD-1 could

bind 94.7% of PD-L1, preventing CTLs dysfunction and failure resulting from the combination of PD-L1 with PD-1 on CTLs. Thus, CTLs can effectively target tumor cells. LOMV@PD-1 treatment reduced the IFN-γ expression in the plasma, maintaining a normal immune microenvironment while not causing excessive damage to the body.

According to the Pearson correlation analysis,[19] the IFN-γ concentration in plasma was positively correlated with plasma PD-L1 concentration (correlation coefficient: 0.8942) (**Figure 6**k). This indicates that the positive antitumor effect of IFN-γ was superior to the negative effect. In addition, IFN-γ in tumor tissue was positively correlated with PD-L1 (correlation coefficient: 0.8303) (**Figure 6**l), which is consistent with a previous report.[19] As shown in **Figure 6**m, the expression of IFN-γ in tumor tissues was negatively correlated with tumor volume, indicating that LOMV@PD-1 effectively shielded the side-effect of IFN-γ from producing PD-L1 and amplified the positive effect of tumor inhibition.

To verify the long-term immune memory effect, we tested the expression of $CD3^+CD8^+CD44^+CD62L^+$ in Tcm cells.[29] The results showed that the number of Tcm cells in the LOMV@PD-1 group increased with the time after treatment and reached 47.13% at day 43, confirming the long-term immune memory effects (**Figure S12**b and **Figure 6**n). This is due to the immune response induced by the outer-membrane proteins in OMVs. The

immune memory effect, along with the high immunogenicity and non-replication, makes OMVs a suitable candidate for vaccine.[30]

Breast cancer exhibits low immunogenicity and has a low response rate in clinical treatment, whereas checkpoint inhibitors have a high response rate in melanoma and a long-lasting effect.[5ab,31] Given the significant antitumor effect on 4T1 tumors, LOMV@PD-1 was tested on mouse melanoma B16 with high immunogenicity[5a] and mouse colorectal cancer CT26 models with low response rate[5b] to verify the universality of tumor inhibition. First, LOMV@PD-1 was administered to B16 tumor-bearing mice. According to the result, LOMV@PD-1 had a good antitumor effect with a tumor inhibition rate of 94.21% and the tumor in one mouse even disappeared completely (**Figure S13**a-c). There were significant differences in tumor volume and weight between the saline group and LOMV@PD-1 group (**Figure 7**a, b), whereas negligible differences were observed in mouse body weight between the groups (**Figure 7**c). Thus, LOMV@PD-1 exerted an excellent antitumor immune response.

To analyze the mechanism of tumor inhibition, ELISA was used to detect PD-L1 expression in tumor tissues. The results showed that the saline group had the lowest PD-L1 expression, whereas the LOMV@PD-1 group had the highest expression (**Figure 7**d), which was consistent with the results obtained for the 4T1 model. This indicates that most of the

PD-L1 was expressed by immune cells (such as DCs, T cells, NK cells, and macrophages), and the expression level of PD-L1 was positively related to the efficacy of immune checkpoint inhibitors. Then, the magnetic particle chemiluminescence kit was used to detect the concentration of PD-1/PD-L1 conjugates and the blocking rate in the LOMV@PD-1 group was calculated to be as high as 96.7% (**Figure 7**e), which was 9.04 times that of the anti-PD-L1+LOMV group, indicating that B16 melanoma was more sensitive to LOMV@PD-1 than the anti-PD-L1 group. Moreover, the IFN-γ expression in tumor tissues was the highest in the optimum group (**Figure 7**f), indicating that LOMV@PD-1 caused the recruitment of immune cells and activated the release of IFN-γ to fight tumors. Immunofluorescence images showed that the LOMV@PD-1 group had more obvious orange fluorescence than the other groups (**Figure 7**g), which further proved the largest combination of PD-1 and PD-L1.

Next, we evaluated whether CTLs and NK cells could produce an immune response. First, the expression of DCs was determined. The results showed that the expression of $CD86^+CD80^+$ DCs in the LOMV@PD-1 group was as high as 65.72 % (**Figure 7**h, i) and that the expressions of $CD4^+$ and $CD8^+$ T cells also increased compared to that in the saline group (**Figure 7**j-l). In addition, the expression level of $CD49b^+$ NK cells in the LOMV@PD-1 group was 2.22 higher than that in the saline group (**Figure 7**m, n). The immunofluorescence images showed the strongest fluorescence in the LOMV@PD-1 group,

indicating that LOMV@PD-1 promoted the expression of CTLs and NK cells to enhance the immune response (**Figure 7**q). Finally, the expression of Tcm cells was detected on day 30. The number of Tcm cells produced by LOMV@PD-1 was 3.66 higher than that produced in the saline group, exhibiting a long-term immune memory effect in the B16 model (**Figure 7**o, p). These results indicated that LOMV@PD-1 exhibited more efficient tumor suppression in the B16 model than the 4T1 tumor, which was mainly due to the excellent blocking rate of B16 tumors with high immunogenicity.

The therapeutic effects were studied using the CT26 model. The tumor inhibition rate of LOMV@PD-1 reached approximately 70%, which was only 44% in the anti-PD-L1+LOMV group (**Figure S14**a-c). Similar to the results obtained for the B16 model, there were significant differences in tumor volume and tumor weight between the saline group and LOMV@PD-1 group (**Figure 8**a, b), whereas no obvious difference was observed in the mouse body weight between the groups (**Figure 8**c).

Next, we analyzed the effects of self-blockade. The results showed that the expressions of PD-L1 in the LOMV@PD-1 and anti-PD-L1+LOMV groups were similar, both of which significantly differed from that of the saline group (**Figure 8**d). The LOMV@PD-1 group had the highest concentration of PD-1/PD-L1 conjugates with a blocking rate of 77.22%, which was 1.4 higher than that of the anti-PD-L1+LOMV group (**Figure 8**e). Furthermore,

LOMV@PD-1 had the highest expression of IFN-γ in tumor tissues (**Figure 8**f). Immunofluorescence staining revealed a superior combination of PD-1 and PD-L1 in the LOMV@PD-1 group compared to the other two groups (**Figure 8**g).

Furthermore, flow cytometry was performed to analyze the expressions of DCs, CTLs, and NK cells, which showed the highest expression of these cells in the LOMV@PD-1 group (**Figure 8**h-o). The immunofluorescence images further confirmed the flow cytometry results (**Figure 8**r). Finally, the expression of Tcm cells was detected on day 30. The results showed that the number of Tcm cells produced by LOMV@PD-1 was 1.45 higher than that produced by the saline group (**Figure 8**p, q). By comparing the antitumor effects of these three models, B16 showed the strongest response to the engineered *E. coli* loading with PD-1 plasmid, followed by 4T1, and finally, the CT26 model.

We successfully developed a LyP1 polypeptide-modified outer-membrane vesicle loaded with a PD-1 plasmid to induce the self-expression of PD-1 by tumor cells. The nanocarriers could be effectively internalized by tumor cells through LyP1 peptide-mediated targeting, showing 1.5-fold tumor accumulation compared to the nontargeted OMV. In particular, tumor cells could express PD-1 after the delivery of PD-1 plasmid to the nucleus by the nanocarriers. Subsequently, the self-expressed PD-1 was bound to PD-L1 expressed by both autologous and neighboring tumor cells to block the PD-1/PD-L1 pathway. The blocking rate

of the nanocarriers was as high as 94.7% in 4T1 tumors and 96.7% in B16 tumors, which were 1.90 and 9.04 times higher than that of the PD-L1 monoclonal antibody, respectively. Moreover, the bacterial outer-membrane vesicles recruited CTLs and NK cells to tumors, inducing the secretion of IFN-γ to fight tumors. The self-blockade of PD-L1 combined with the requirement of immune cells resulted in remarkable antitumor efficiency of nanocarriers against various tumors, especially showing the strongest response of B16 tumors with a tumor inhibition rate of 94.21%, which was 1.47-fold that of the monoclonal antibody therapy. Therefore, this simple and safe strategy paves way in the development of nanomedicines for tumor immunotherapy.

Supporting Information

Supporting Information is available from the Wiley Online Library or from the author.

Acknowledgements

This work was partially supported by National Natural Science Foundation of China (51725303, 52033007, 52073236) and the 5th Chinese Association for Science and Technology Young Talents Support Project. The authors thank Analytical and Testing Center of Southwest Jiaotong University.

Received: ((will be filled in by the editorial staff))
Revised: ((will be filled in by the editorial staff))
Published online: ((will be filled in by the editorial staff))

References

[1] a) D. M. Pardoll, *Nat. Rev. Cancer* **2012**, *12*, 252; b) S. C. Wei, J. H. Levine, A. P. Cogdill, Y. Zhao, N.-A. A. S. Anang, M. C. Andrews, P. Sharma, J. Wang, J. A. Wargo, D. Pe'er, J. P. Allison, *Cell* **2017**, *170*, 1120; c) S. L. Topalian, J. M. Taube, D. M. Pardoll, *Science* **2020**, *367*, eaax0182.

[2] a) S. Koyama, E. A. Akbay, Y. Y. Li, G. S. Herter-Sprie, K. A. Buczkowski, W. G. Richards, L. Gandhi, A. J. Redig, S. J. Rodig, H. Asahina, R. E. Jones, M. M. Kulkarni, M. Kuraguchi, S. Palakurthi, P. E. Fecci, B. E. Johnson, P. A. Janne, J. A. Engelman, S. P. Gangadharan, D. B. Costa, G. J. Freeman, R. Bueno, F. S. Hodi, G. Dranoff, K. K. Wong, P. S. Hammerman, *Nat. Commun.* **2016**, *7*, 10501; b) H. Nishimura, M. Nose, H. Hiai, N. Minato, T. Honjo, *Immunity* **1999**, *11*, 141.

[3] a) M. E. Keir, M. J. Butte, G. J. Freeman, A. H. Sharpe, *Annu. Rev. Immunol*. **2008**, *26*, 677; b) T. Okazaki, T. Honjo, *Trends Immunol*. **2006**, *27*, 195; c) A. Ribas, J. D. Wolchok, *Science* **2018**, *359*, 1350.

[4] P. Sharma, J. P. Allison, *Science* **2015**, *348*, 56.

[5] a) F. S. Hodi, S. J. O'Day, D. F. McDermott, R. W. Weber, J. A. Sosman, J. B. Haanen, R. Gonzalez, C. Robert, D. Schadendorf, J. C. Hassel, W. Akerley, A. J. M. van den Eertwegh, J. Lutzky, P. Lorigan, J. M. Vaubel, G. P. Linette, D. Hogg, C. H. Ottensemier, C. Leebé, C. Peschel, I. Quirt, J. I. Clark, J. D. Wolchok, J. S. Weber, J. Tian, M. J. Yellin, G. M. Nichol, A. Hoos, W. J. Urba, *N. Engl. J. Med*. **2010**, *363*, 711; b) P. Sharma, S. Hu-Lieskovan, J. A. Wargo, A. Ribas, *Cell* **2017**, *168*, 707; c) P. Sasikumar, R. Shrimali, S. Adurthi, R.

Ramachandra, L. Satyam, A. Dhudashiya, D. Samiulla, K. B. Sunilkumar, M. Ramachandra, *J. Immunother. Cancer* **2013**, *1*, O24.

[6] JM. Chinai, M. Janakiram, F. Chen, W. Chen, M. Kaplan, X. Zang, *Trends Pharmacol Sci*. **2015**, *36*, 587.

[7] a) D. Schmid, C. G. Park, C. A. Hartl, N. Subedi, A. N. Cartwright, R. B. Puerto, Y. Zheng, J. Maiarana, G. J. Freeman, K. W. Wucherpfennig, D. J. Irvine, M. S. Goldberg, *Nat. Commun*. **2017**, *8*, 1747; b) D. Wang, T. Wang, H. Yu, B. Feng, L. Zhou, F. Zhou, B. Hou, H. Zhang, M. Luo, Y. Li, *Sci. Immunol*. **2019**, *4*, eaau6584; c) A. K. Kosmides, J.-W. Sidhom, A. Fraser, C. A. Bessell, J. P. Schneck, *ACS Nano* **2017**, *11*, 5417; d) C. Wang, W. Sun, G. Wright, A. Z. Wang, Z. Gu, *Adv. Mater*. **2016**, *28*, 8912.

[8] H. Phuengkham, L. Ren, I. W. Shin, Y. T. Lim, *Adv. Mater*. **2019**, *31*, 1803322.

[9] C. He, X. Duan, N. Guo, C. Chan, C. Poon, R. R. Weichselbaum, W. Lin, *Nat. Commun*. **2016**, *7*, 12499.

[10] C. T.-S. Victor, A. J. Rech, A. Maity, R. Rengan, K. E. Pauken, E. Stelekati, J. L. Benci, B. H. Xu, H. Dada, P. M. Odorizzi, R. S. Herati, K. D. Mansfield, D. Patsch, R. K. Amaravadi, L. M. Schuchter, H. Ishwaran, R. Mick, D. A. Pryma, X. W. Xu, M. D. Feldman, T. C. Gangadhar, S. M. Hahn, E. J. Wherry, R. H. Vonderheide, A. J. Minn, *Nature* **2015**, *520*, 373.

[11] Q. Chen, L. Xu, C. Liang, C. Wang, R. Peng, Z. Liu, *Nat. Commun*. **2016**, *7*, 13193.

[12] a) Q. Chen, H. Bai, W. Wu, G. Huang, Y. Li, M. Wu, G. Tang, Y. Ping, *Nano Lett*. **2020**, *20*, 11; b) X. Huang, J. Pan, F. Xu, B. Shao, Y, Wang, X. Guo, S. Zhou, *Adv. Sci*. **2020**, *8*, 2003572.

[13] O. Y. Kim, H. T. Park, N. T. H. Dinh, S. J. Choi, J. Lee, J. H. Kim, S. W. Lee, Y. S. Gho, *Nat. Commun*. **2017**, *8*, 626.

[14] B. W. Simpson, M. S. Trent, *Nat. Rev. Microbiol*. **2019**, *17*, 403.

[15] a) W. Song, A. C. Anselmo, L. Huang, *Nat. Nanotechnol*. **2019**, *14*, 1093; b) W. Song, K. Tiruthani, Y. Wang, L. Shen, M. Hu, O. Dorosheva, K. Qiu, K. A. Kinghorn, R. Liu, L. Huang, *Adv. Mater*. **2018**, *30*, e1805007.

[16] a) S. N. Wai, B. Lindmark, T. Söderblom, A. Takade, M. Westermark, J. Oscarsson, J. Jass, A. Richter-Dahlfors, Y. Mizunoe, B. E. Uhlin, *Cell* **2003**, *115*, 25; b) V. Gujrati, S. Kim, S.-H. Kim, J. J. Min, H. E. Choy, S. C. Kim, S. Jon, *ACS Nano* **2014**, *8*, 1525.

[17] J. M. Kinsella, R. E. Jimenez, P. P. Karmali, A. M. Rush, V. R. Kotamraju, N. C. Gianneschi, E. Ruoslahti, D. Stupack, M. J. Sailor, *Angew. Chemie. Int. Ed*. **2011**, *50*, 12308.

[18] J. Y. Chen, L. S. Penn, J. Xi, *Biosens. Bioelectron*. **2018**, *99*, 593.

[19] G. Chen, A. C. Huang, W. Zhang, G. Zhang, M. Wu, W. Xu, Z. Yu, J. Yang, B. Wang, H. Sun, H. Xia, Q. Man, W. Zhong, L. F. Antelo, B. Wu, X. Xiong, X. Liu, L. Guan, T. Li, S. Liu, R. Yang, Y. Lu, L. Dong, S. M. Gettigan, R. Somasundaram, R. Radhakrishnan, G. Mills, Y. Lu, J. Kim, Y. H. Chen, H. Dong, Y. Zhao, G. C. Karakousis, T. C. Mitchell, L. M. Schuchter, M. Herlyn, E. J. Wherry, X. Xu, W. Guo, *Nature* **2018**, *560*, 382.

[20] a) D. Villalta, P. Martelli, A. Moratto, E. Ligato, R. Giacomello, S. EI. I. EI. Hachimi, *J. Clin. Microbiol*. **2020**, *58*, e01436; b) M. Goto, K. Chamoto, K. Higuchi, S. Yamashita, K. Noda, T. Iino, M. Miura, T. Yamasaki, O. Ogawa, M. Sonobe, H. Date, J. Hamanishi, M. Mandai, Y. Tanaka, S. Chikuma, R. Hatae, M. Muto, S. Minamiguchi, N. Minato, T. Honjo, S*ci. Rep*. **2019**, *9*, 10144.

[21] R. Ge, C. Liu, X. Zhang, W. Wang, B. Li, J. Liu, Y. Liu, H. Sun, D. Zhang, Y. Hou, H. Zhang, B. Yang, *ACS Appl. Mater. Interfaces* **2018**, *10*, 20342.

[22] R. Zhang, Z. Zhu, H. Lv, F. Li, S. Sun, J. Li, C.-S. Lee, *Small* **2019**, *15*, 1903881.

[23] F. Xu, X. Li, X. Huang, J. Pan, Y. Wang, S. Zhou, *Sci. Adv*. **2020**, *6*, eabb8725.

[24] a) Y. Okuma, H. Wakui, H. Utsumi, Y. Sagawa, Y. Hosomi, K. Kuwano, S. Homma, *Clin Lung Cancer* **2018**, *19*, 410; b) P. Hofman, S. Heeke, C. Alix-Panabières, K. Pantel, *Ann. Oncol*. **2019**, *30*, 1448.

[25] a) J. Gao, L. Z. Shi, H. Zhao, J. Chen, L. Xiong, Q. He, T. Chen, J. Roszik, C. Bernatchez, S. E. Woodman, P.-L. Chen, P. Hwu, J. P. Allison, A. Futreal, J. A. Wargo, P. Sharma, *Cell* **2016**, *167*, 397; b) L. C. Platanias, *Nat. Rev. Immunol*. **2005**, *5*, 375.

[26] a) A. Garcia-Diaz, D. S. Shin, B. H. Moreno, J. Saco, H. Escuin-Ordinas, G. A. Rodriguez, J. M. Zaretsky, L. Sun, W. Hugo, X. Wang, G. Parisi, C. P. Saus, D. Y. Torrejon, T. G. Graeber, B. Comin-Anduix, S. Hu-Lieskovan, R. Damoiseaux, R. S. Lo, A. Ribas, *Cell Rep*. **2017**, *19*, 1189; b) C. Sun, R. Mezzadra, T. N. Schumacher, *Immunity* **2018**, *48*, 434.

[27] Y. Li, R. Zhao, K. Cheng, K. Zhang, Y. Wang, Y. Zhang, Y. Li, G. Liu, J. Xu, J. Xu, G. Anderson, J. Shi, L. Ren, X. Zhao, G. Nie, *ACS Nano* **2020**, *14*, 16698.

[28] D. Dangaj, M. Bruand, A. J. Grimm, C. Ronet, D. Barras, P. A. Duttagupta, E. Lanitis, J. Duraiswamy, J. L. Tanyi, F. Benencia, J. Conejo-Garcia, H. R. Ramay, K. T. Montone, D. J. Powell Jr., P. A. Gimotty, A. Facciabene, D. G. Jackson, J. S. Weber, S. J. Rodig, S. F. Hodi, L. E. Kandalaft, M. Irving, L. Zhang, P. Foukas, S. Rusakiewicz, M. Delorenzi, G. Coukos, *Cancer Cell* **2019**, *35*, 885.

[29] L. Zhang, J. Zhou, L. Hu, X. Han, X. Zou, Q. Chen, Y. Chen, Z. Liu, C. Wang, *Adv. Funct. Mater*. **2020**, *30*, 1906922.

[30] a) K. Cheng, R. Zhao, Y. Li, Y. Qi, Y. Wang, Y. Zhang, H. Qin, Y. Qin, L. Chen, C. Li, J. Liang, Y. Li, J. Xu, X. Han, G. J. Anderson, J. Shi, L. Ren, X. Zhao, G. Nie, *Nat. Commun*. **2021**, *12*, 2041; b) M. F. Bachmann, G. T. Jennings, *Nat. Rev. Immunol*. **2010**, *10*, 787.

[31] a) R. Brahmer, S. S. Tykodi, L. Q. M. Chow, W.-J. Hwu, S. L. Topalian, P. Hwu, C. G. Drake, L. H. Camacho, J. Kauh, K. Odunsi, H. C. Pitot, O. Hamid, S. Bhatia, R. Martins, K. Eaton, S. Chen, T. M. Salay, S. Alaparthy, J. F. Grosso, A. J. Korman, S. M. Parker, S. Agrawal, S. M. Goldberg, D. M. Pardoll, A. Gupta, J. M. Wigginton, *N. Engl. J. Med*. **2012**, *366*, 2455; b) S. L. Topalian, F. S. Hodi, J. R. Brahmer, S. N. Gettinger, D. C. Smith, D. F. McDermott, J. D. Powderly, R. D. Carvajal, J. A. Sosman, M. B. Atkins, P. D. Leming, D. R. Spigel, S. J. Antonia, L. Horn, C. G. Drake, D. M. Pardoll, L. Chen, W. H. Sharfman, R. A. Anders, J. M. Taube, T. L. McMiller, H. Xu, A. J. Korman, M. Jure-Kunkel, S. Agrawal, D. M. Donald, G. D. Kollia, A. Gupta, J. M. Wigginton, M. Sznol, *N. Engl. J. Med*. **2012**, *366*, 2443.

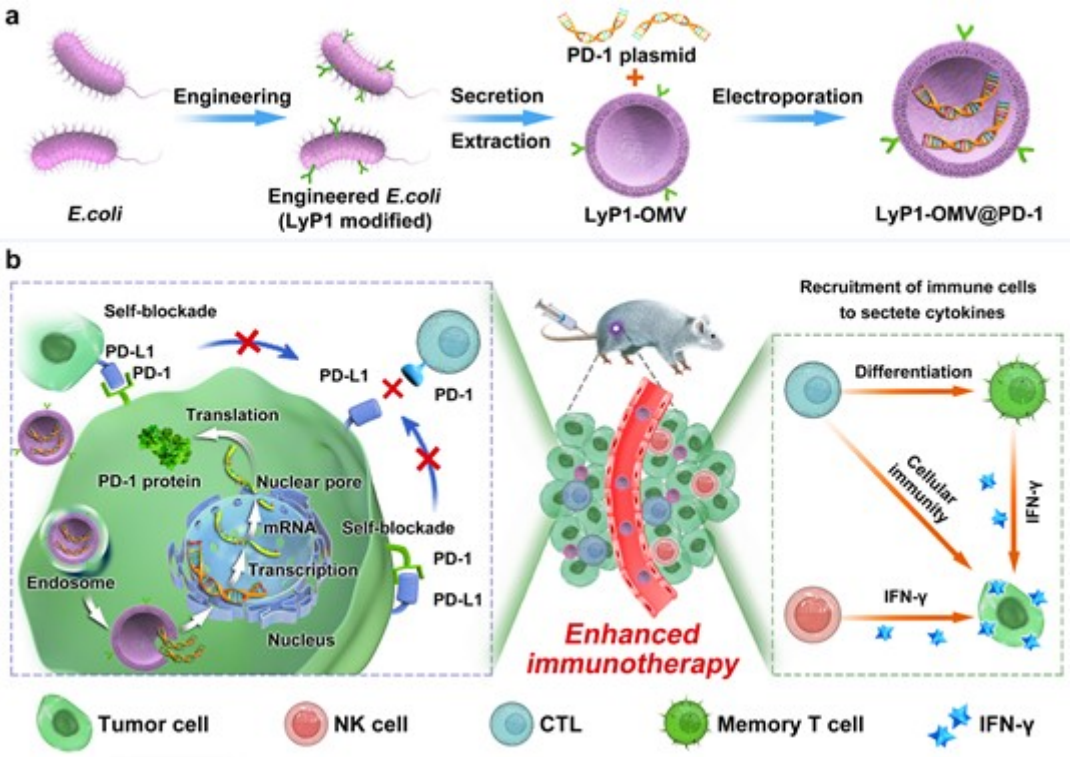

Figure 1. Schematic of tumor immunotherapy mediated by LOMV@PD-1 nanoparticles. a) The preparation process of LOMV@PD-1 nanoparticle-attenuated *E. coli* was genetically engineered to express tumor-targeted peptide LyP1, and then, the OMVs were extracted and loaded with PD-1 plasmid by electroporation to fabricate LOMV@PD-1. b) LOMV@PD-1 targeted the tumor cells via LyP1-mediated endocytosis and released PD-1 plasmid in the nucleus, resulting in the expression of PD-1 by tumor cells, which bonded to the intrinsic PD-L1, blocking the PD-1/PD-L1 pathway and preventing the immune escape. The OMVs recruited CTLs and NK cells to the tumor microenvironment and induced the secretion of INF-γ to enhance the immune effect of anti-PD-1/PD-L1 treatment.

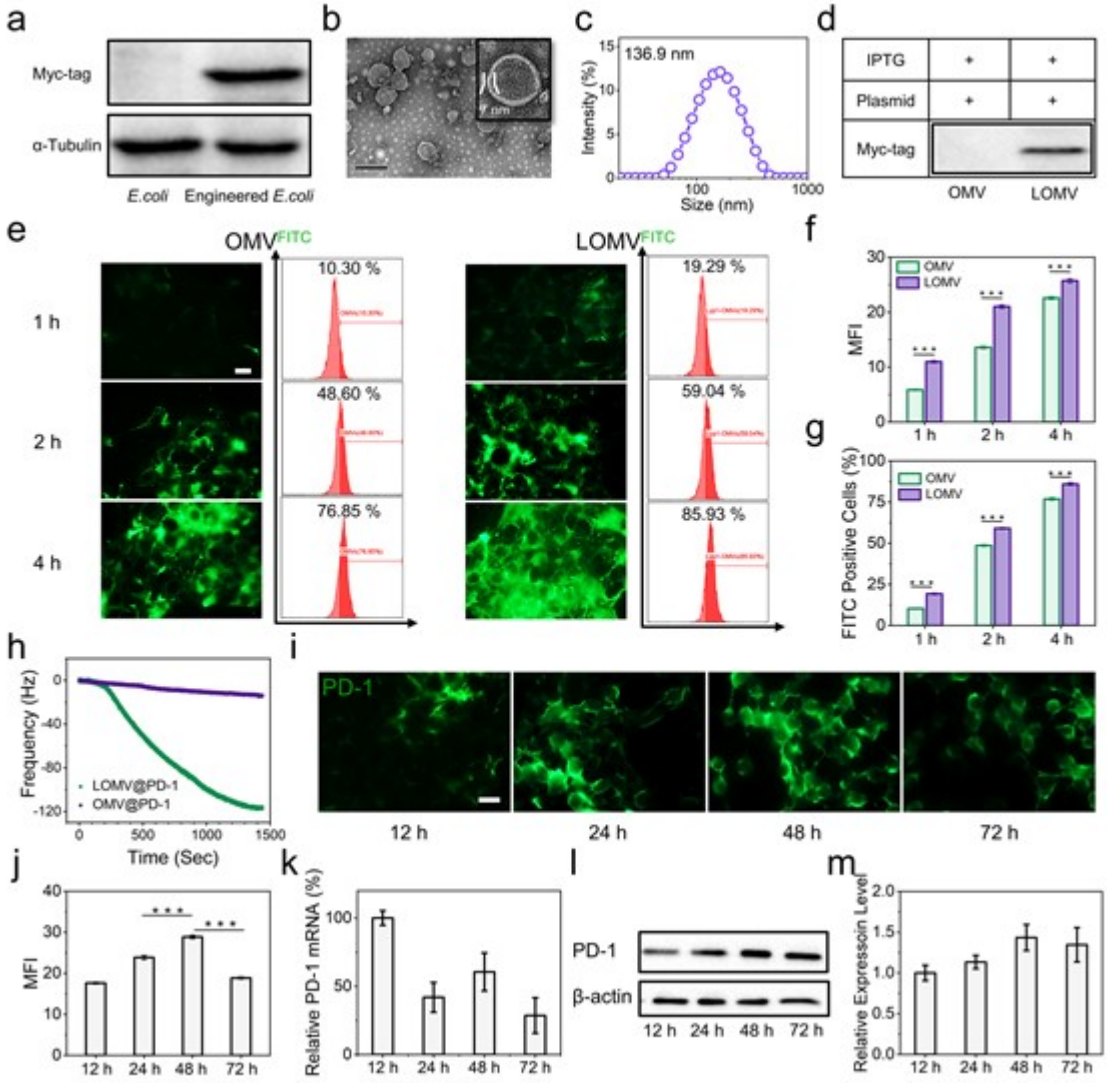

Figure 2. Characterization and targeting validation of LOMV, and expression of PD-1 after transfection with plasmid. a) Western blotting confirmed the localization of LyP1 in engineered *E. coli*. b) Transmission electron micrograph image of *E. coli* K-12 W3110-derived LOMV. Scale bars, 200 nm. c) Size distribution of *E. coli* K-12 W3110 measured by dynamic light scattering analysis (n = 5). d) Western blotting analysis of ClyA-LyP1 in OMV. LOMV means LyP1-OMV. e) Fluorescence images and f, g) flow cytometry results of 4T1 cells after incubation with OMV and LOMV at different time points (Scale bar = 20

μm). h) Quartz crystal microbalance analyses of targeting tumor cell effects of LOMV and OMV. i) Fluorescence microscope showing the expression of PD-1 in 4T1 cells at 12, 24, 48, and 72 h. (Scale bar = 20 μm). j) Mean fluorescence intensity quantification of PD-1 expression. k) Relative PD-1 mRNA expression determined by quantitative real-time polymerase chain reaction. l) PD-1 protein expression determined by western blotting. m) Quantitative analysis of light intensities of relative PD-1 protein expression obtained from western blotting results. *$P < 0.05$, **$P < 0.01$, ***$P < 0.001$.

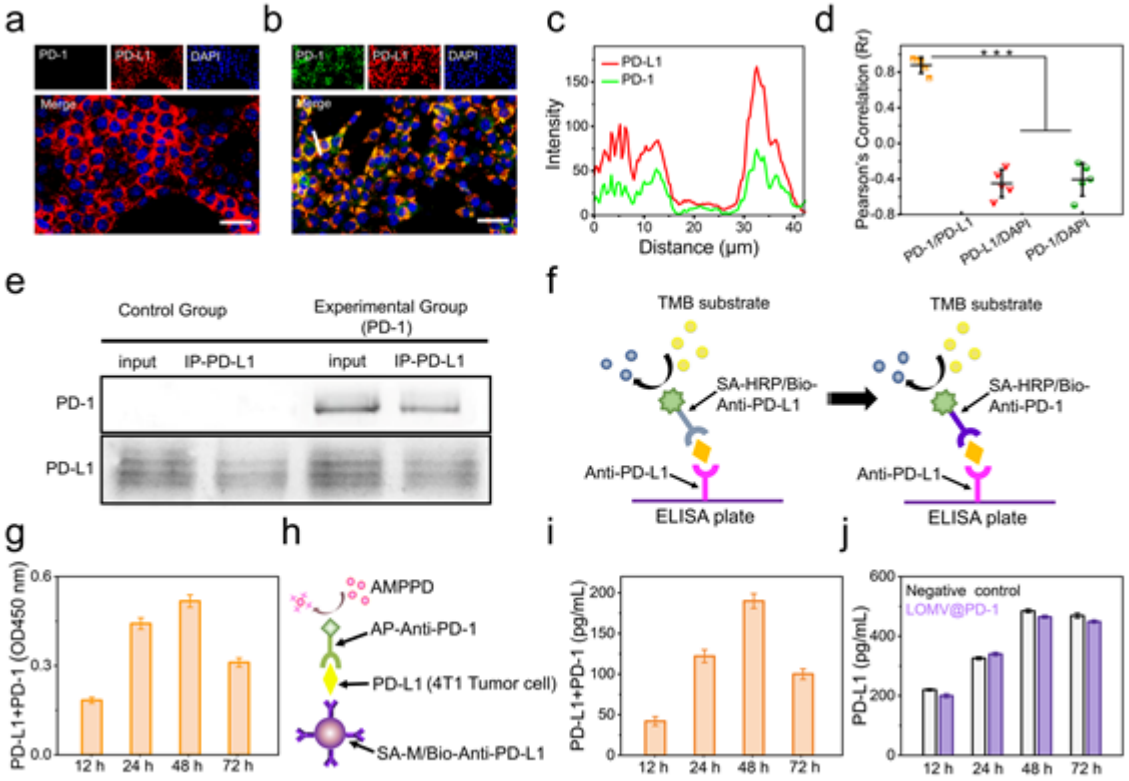

Figure 3. Verification of the combination of PD-1 and PD-L1. Fluorescence images showing the expressions of PD-L1 and PD-1 in 4T1 cells without treatment a) or of those treated with LOMV@PD-1 for 48 h b) PD-1 was labeled with green fluorescence, PD-L1 was labeled with red fluorescence, and nuclei were stained with DAPI (blue) (Scale bar = 50 μm). c) Intensity of the underline part in Figure b, showing PD-1/PD-L1 colocalization. d) Pearson's correlation coefficient of the merged fluorescence from Figure b (n = 5, ***P < 0.001). e) PD-1/PD-L1 combination test by co-immunoprecipitation assay. f-g) Schematic (left) of ELISA to measure PD-L1 concentration. Schematic (right) of modified ELISA to measure the OD value of PD-1/PD-L1 conjugates. TMB, 3,3′,5,5′-tetramethylbenzidine; SA-HRP, streptavidin-horseradish peroxidase. h-i) Principle and results of the detection of PD-1/PD-L1 conjugates' concentration by magnetic particle chemiluminescence method. j) The ELISA method on the left of Figure f) is used to detect the PD-L1 concentration.

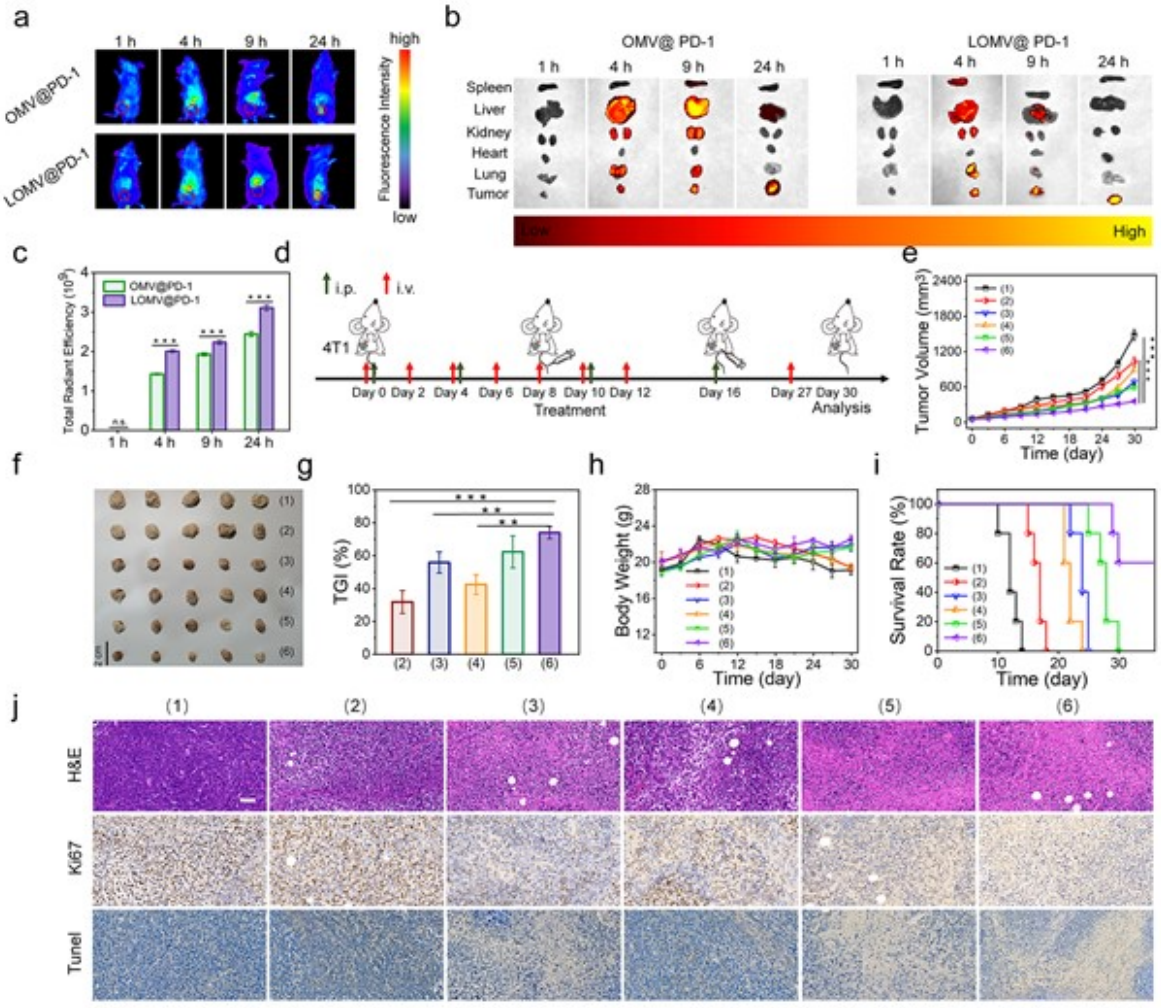

Figure 4. Biodistribution and *in vivo* antitumor effect. a) *In vivo* fluorescence images of 4T1 tumor-bearing mice at 1, 4, 9, and 24 h post tail vein injection of LOMV and OMV. The red circles indicate the tumor site. b) *Ex vivo* imaging showing the distribution of LOMV and OMV in the spleen, liver, kidney, heart, lung, and tumor site 24 h post injection. c) Semi-quantification of vesicles in the tumors based on Cy5.5 fluorescence intensity. d) Treatment schedule for 4T1 breast tumor bearing BALB/c mice. Red arrow indicates intravenous injection of saline and vesicles with or without PD-1 plasmid encapsulation; green arrow indicates intraperitoneal injection of anti-PD-L1. e) Tumor volume. (1) Saline, (2) Anti-PD-L1, (3) Anti-PD-L1+LOMV, (4) LOMV, (5) OMV@PD-1, and (6) LOMV@PD-1. f) Photographs of the excised tumors from the mice on day 30. g) TGI on day 30. TGI (%) = (mean tumor weight of control group-mean tumor weight of experimental group)/mean tumor

weight of control group × 100. h) Body weight and i) survival curves of the different treatment groups. j) H&E staining, Ki67 analysis, and TUNEL assay of tumor sections after treatment (scale bar = 50 μm). In H&E staining, nuclei are stained blue and the extracellular matrix and cytoplasm are stained red. Both Ki67-positive proliferating cells and TUNEL-positive apoptotic cells are stained brown. All statistical data are presented as mean ± standard deviation (n = 5; *$p < 0.05$, **$p < 0.01$, ***$p < 0.001$).

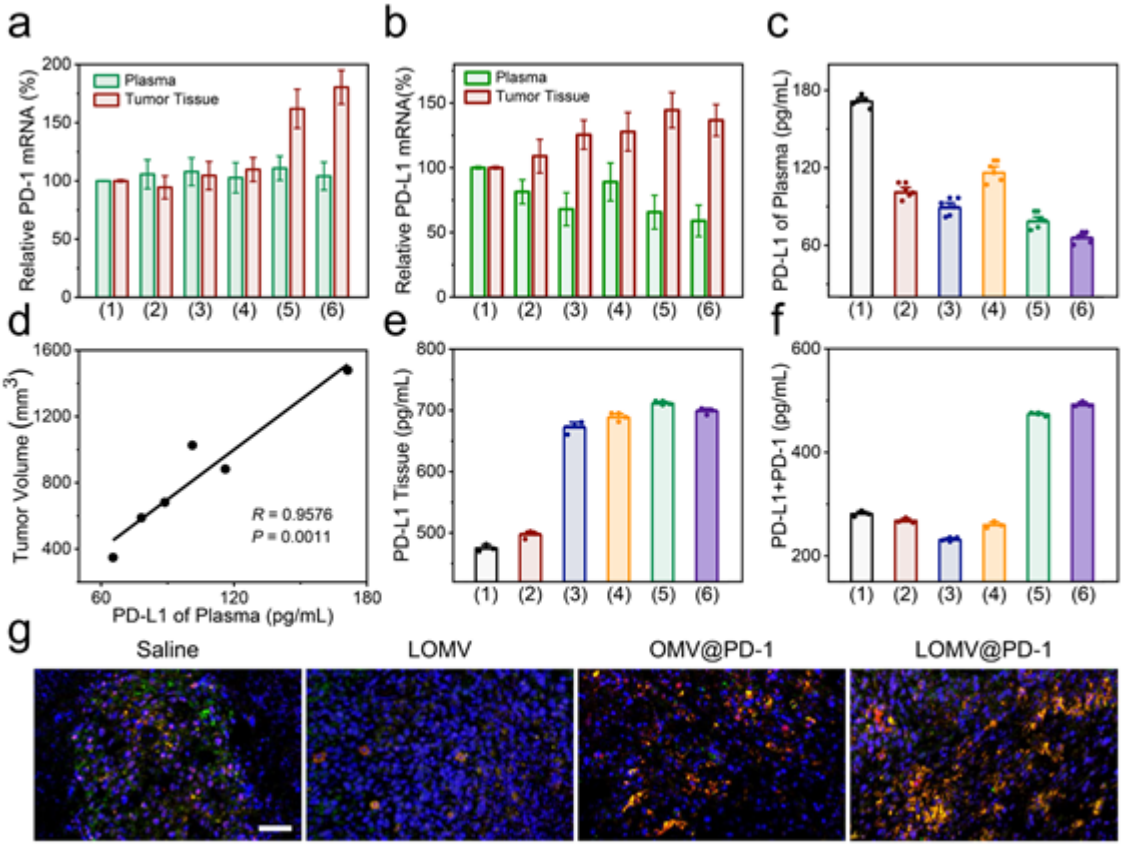

Figure 5. Blockade of PD-L1 *in vivo*. a, b) Relative mRNA levels of PD-1 and PD-L1 by qPCR. c) PD-L1 expression in plasma by ELISA. (1) Saline, (2) Anti-PD-L1, (3) Anti-PD-L1+LOMV, (4) LOMV, (5) OMV@PD-1, (6) LOMV@PD-1. d) Pearson correlation between the PD-L1 concentration in plasma and tumor burden in 4T1-bearing mice. e) PD-L1 expression in 4T1 tumor by ELISA. f) Concentration of PD-1/PD-L1 conjugates in mouse tumor tissues by magnetic particle chemiluminescence method. g) Immunofluorescence of PD-1/PD-L1 co-localization in tumor tissues. PD-1 was labeled with green fluorescence and PD-L1 was labeled with red fluorescence (scale bar = 50 μm).

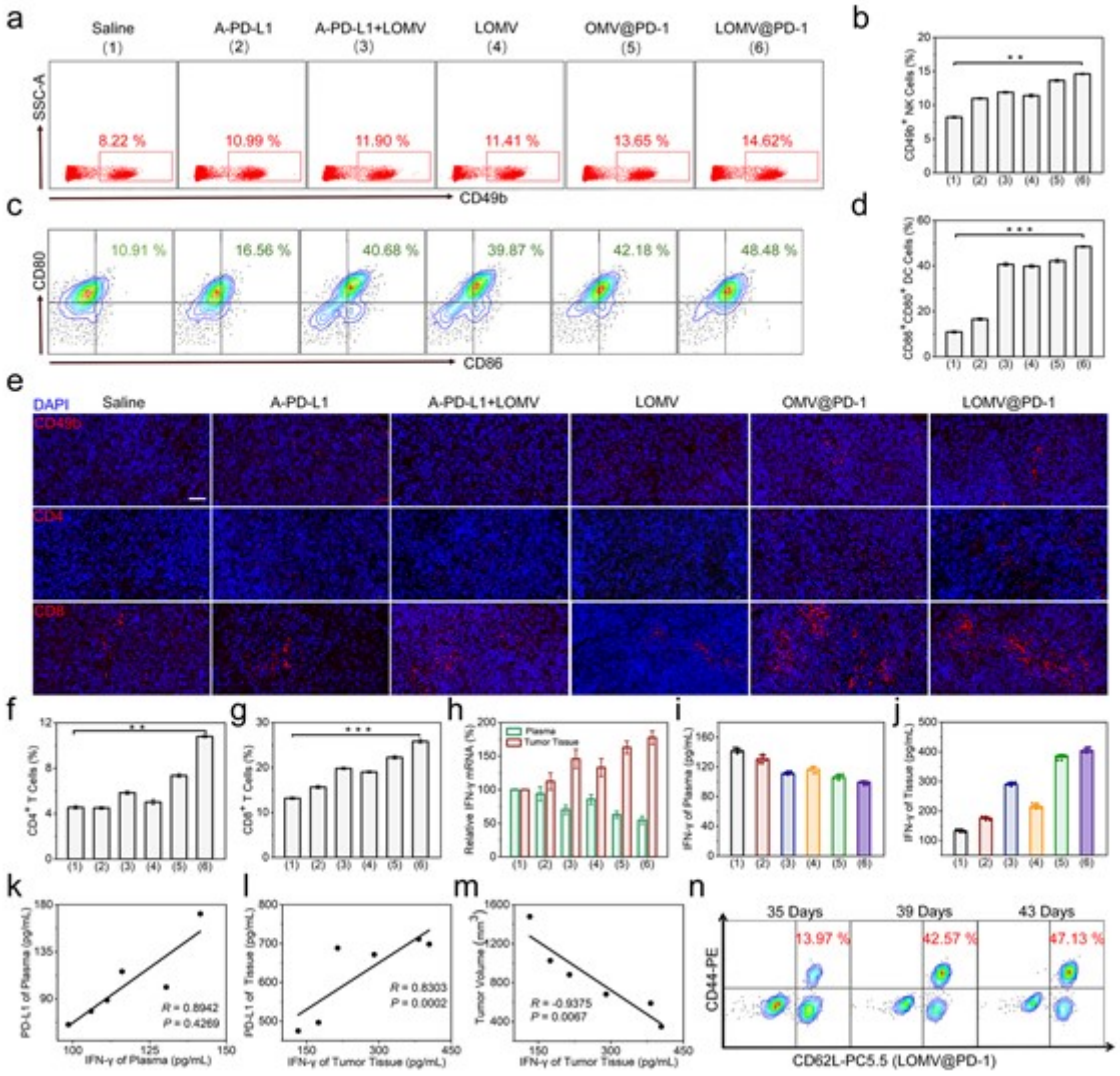

Figure 6. Recruitment and activation of immune cells. a, b) Flow cytometry analysis of $CD49b^+$ NK cells in the tumor tissues at the end of the treatments. (1) Saline, (2) Anti-PD-L1, (3) Anti-PD-L1+LOMV, (4) LOMV, (5) OMV@PD-1, (6) LOMV@PD-1. c, d) Representative flow cytometry scatter plots of the percentage of $CD80^+CD86^+$ DCs from the lymph nodes. e) Immunofluorescence staining of $CD49b^+$, $CD4^+$, and $CD8^+$ cells (red) in tumor tissues (scale bar = 50 μm). f, g) Quantification of $CD4^+$ and $CD8^+$ T cells in the tumor tissues. h) Relative mRNA levels of INF-γ by qPCR. i, j) The expression of INF-γ in plasma and tumor tissue. k, l) Pearson correlation between the INF-γ and PD-L1 in plasma and tumor tissues. m) Pearson correlation between the INF-γ in tumor tissue and tumor burden. n) Flow

cytometry analysis of Tcm cells in the blood of mice treated by LOMV@PD-1 on day 35, 39 and 43.

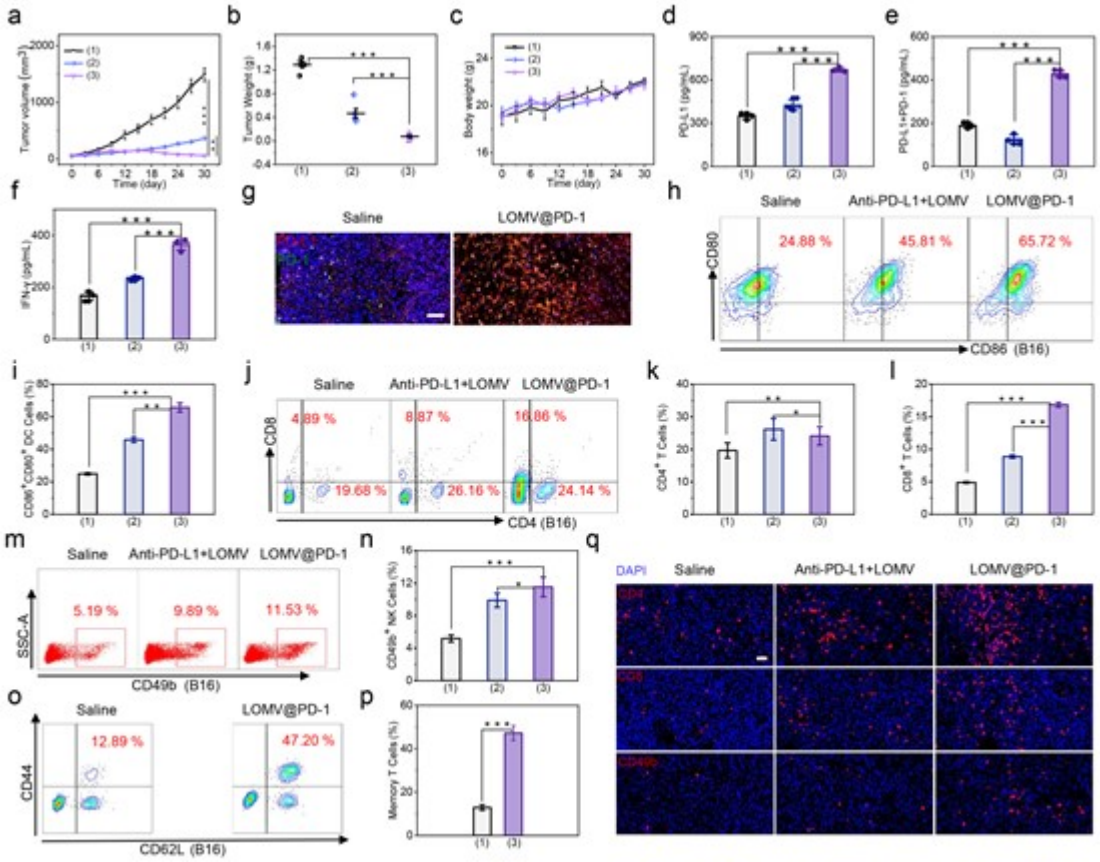

Figure 7. Anti-B16 tumor activity of (1) Saline, (2) Anti-PD-L1+LOMV, and (3) LOMV@PD-1. a) Tumor volume, b) Tumor weight, and c) body weight of the different treatment groups. d) Expression of PD-L1 in tumors. e) Concentration of PD-1/PD-L1 conjugates in tumors by magnetic particle chemiluminescence method. f) Expression of INF-γ in tumors by ELISA. g) Immunofluorescence of PD-1/PD-L1 co-localization in tumors. PD-1 was labeled with green fluorescence and PD-L1 was labeled with red fluorescence (scale bar = 50 μm). h, i) Representative flow cytometry scatter plots of the percentage of $CD80^+CD86^+$ DCs from the lymph nodes. j, k, l) Flow cytometry analysis of $CD8^+$ and $CD4^+$ T cells in the tumor tissues at the end of treatments. m, n) Flow cytometry analysis of $CD49b^+$ NK cells in the tumor tissues. o, p) Flow cytometry analysis of Tcm cells in the blood of mice treated with saline and LOMV@PD-1 on day 30. q) Immunofluorescence staining of $CD49b^+$, $CD4^+$, and $CD8^+$ cells (red) in tumor tissues (scale bar = 50 μm).

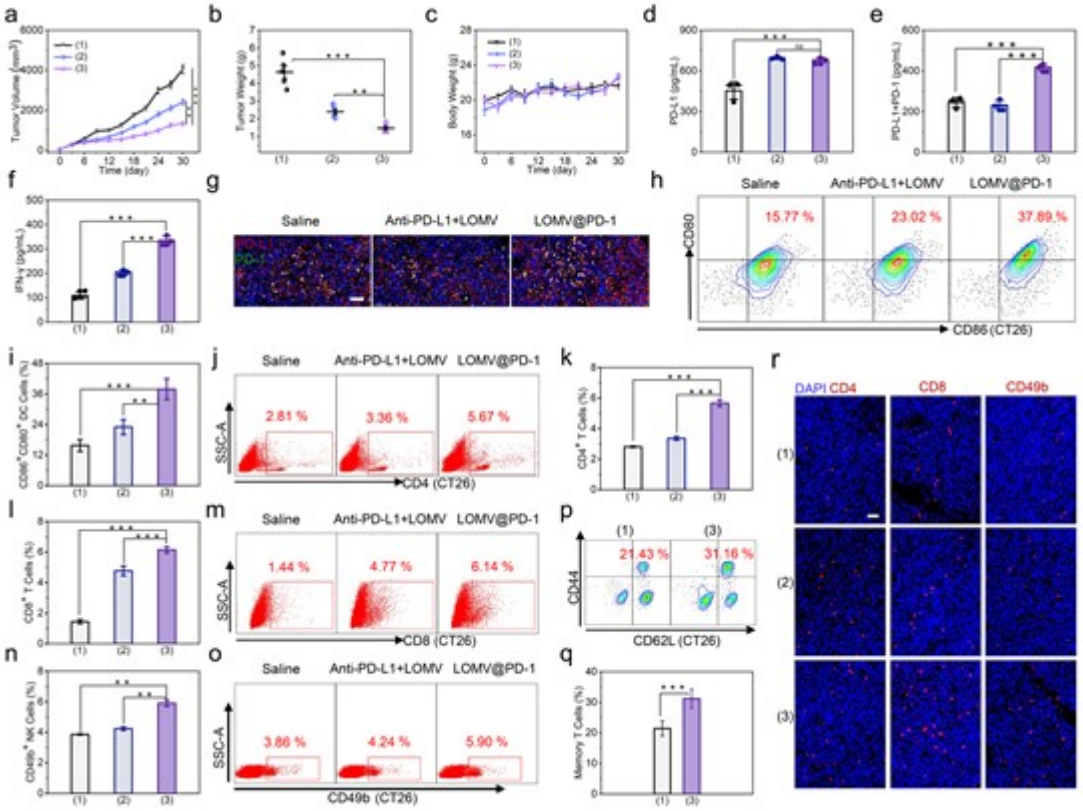

Figure 8. Anti-CT26 tumor activity of (1) Saline, (2) Anti-PD-L1+LOMV, and (3) LOMV@PD-1. a) Tumor volume, b) tumor weight, and c) body weight of the different treatment groups. d) Expression of PD-L1 in tumors. e) Concentration of PD-1/PD-L1 conjugates in tumors by magnetic particle chemiluminescence method. f) Expression of INF-γ in tumors by ELISA. g) The immunofluorescence of PD-1/PD-L1 co-localization in tumors. PD-1 was labeled with green fluorescence and PD-L1 was labeled with red fluorescence (scale bar = 50 μm). h, i) Representative flow cytometry scatter plots of the percentage of $CD80^+CD86^+$ DC cells from the lymph nodes. j, k, l, m) Flow cytometry analysis of $CD8^+$ and $CD4^+$ T cells in the tumor tissues at the end of treatments. n, o) Flow cytometry analysis of $CD49b^+$ NK cells in the tumor tissues. p, q) Flow cytometry analysis of Tcm cells in the blood of mice treated by saline and LOMV@PD-1 on day 30. r) Immunofluorescence staining of $CD49b^+$, $CD4^+$, and $CD8^+$ cells (red) in tumor tissues (scale bar = 50 μm).

The table of contents

A LyP1 polypeptide-modified outer-membrane vesicle loaded with a PD-1 plasmid is developed for inducing the self-expression of PD-1 by tumor cells and achieving self-blockade of the PD-1/PD-L1 pathway. The outer-membrane protein component can recruit cytotoxic lymphocyte cells and natural killer cells to tumor microenvironment, further improving the antitumor activity of the PD-1/PD-L1 self-blocking therapy.

Keywords: immune checkpoint, nanocarrier, outer-membrane vesicle, immunotherapy, immune response

*Jingmei Pan, Xilin Li, Binfen Shao, Funeng Xu, Xuehui Huang, Xing Guo*and Shaobing Zhou**

Self-blockade of PD-L1 with bacteria-derived outer-membrane vesicle for enhanced cancer immunotherapy

ToC figure